

Probing the Neutral Fraction of the IGM with GRBs during the Epoch of Reionisation

Matthew McQuinn^{1*}, Adam Lidz¹, Matias Zaldarriaga^{1,2}, Lars Hernquist¹,
Suvendra Dutta¹

¹ *Harvard-Smithsonian Center for Astrophysics, 60 Garden St., Cambridge, MA 02138*

² *Jefferson Laboratory of Physics, Harvard University, Cambridge, MA 02138*

27 May 2019

ABSTRACT

We show that near-infrared observations of the red side of the $\text{Ly}\alpha$ line from a single gamma ray burst (GRB) afterglow cannot be used to constrain the global neutral fraction of the intergalactic medium (IGM), \bar{x}_H , at the GRB's redshift to better than $\delta\bar{x}_H \sim 0.3$, because some GRB sight-lines will encounter more neutral hydrogen than others owing to the patchiness of reionisation. Consequently, GRBs during the epoch of reionisation will often bear no discernible signature of a neutral IGM in their afterglow spectra. We discuss the constraints on \bar{x}_H from the $z = 6.3$ burst, GRB050904, and quantify the probability of detecting a neutral IGM using future spectroscopic observations of high-redshift, near-infrared GRB afterglows. Assuming an observation with signal-to-noise similar to the Subaru FOCAS spectrum of GRB050904, that the column density distribution of damped $\text{Ly}\alpha$ absorbers is the same as measured at lower redshifts, and that the redshift of the GRB is known, a GRB from an epoch when $\bar{x}_H = 0.5$ can be used to detect a partly neutral IGM at 98% confidence level $\approx 5\text{--}10\%$ of the time (and, for an observation with three times the sensitivity, $\approx 25\text{--}30\%$ of the time).

Key words: cosmology: theory – intergalactic medium – galaxies: high redshift

1 INTRODUCTION

Tomorrow, a gamma ray burst (GRB) may be observed that originates from the death of one of the first stars, during the epoch of reionisation. Despite the great distance to this burst, it will be the brightest gamma ray source on the sky for several tens of seconds, one of the brightest cosmological X-ray sources for hours, and its afterglow will be observable for weeks in the near-infrared (and, for the first day, more than 100 times brighter than any $z \sim 6$ QSO). Much of the optical and near-infrared light will be obscured by the $\text{Ly}\alpha$ forest, and this obscuration will enable the strongest constraint to date on the neutral hydrogen fraction of the intergalactic medium (IGM) at the burst's redshift.

In fact, such an occurrence may already have been realised. Haislip et al. (2006), Kawai et al. (2005), Tagliaferri et al. (2005), and Totani et al. (2006) observed and analysed the optical/near-infrared afterglow of GRB050904, identified to be at $z = 6.3$ – possibly during

the reionisation epoch and the GRB with the highest confirmed redshift. Totani et al. (2006) derived the constraint on the global neutral fraction $\bar{x}_H < 0.6$ at $z = 6.3$. In this paper, we discuss the assumptions that went into their analysis, and we investigate how realistic modelling of reionisation can affect constraints on \bar{x}_H from GRB050904 and from future $z > 6$ GRBs.

The Swift satellite has greatly increased the sample of GRBs with known redshifts in the last two years.¹ Future missions such as EXIST (Grindlay & The Exist Team 2006) and JWST (Gardner et al. 2006) will further enhance our ability to detect high-redshift GRBs and will enable more detailed follow-up studies of their near-infrared afterglows. Interestingly, approximately one-half of Swift bursts are “dark bursts” – bursts that have detected X-ray afterglows, but have no measurable optical emission (e.g., Fillard et al. 2006). While it is probable that most dark bursts are low-redshift, dust-rich galaxies, a fraction of dark bursts may be from $z > 6$ and are “dark” because $\text{Ly}\alpha$ absorption

* mmcquinn@cfa.harvard.edu

¹ http://www.nasa.gov/mission_pages/swift/main/

from the high-redshift IGM erases optical transmission (e.g., Malesani et al. 2005).

In addition to their extreme luminosity, there are several other advantages to studying reionisation with GRBs compared to other probes of the high-redshift Universe. First, the afterglows of high-redshift GRBs are observed at earlier (brighter) times in the source frame than those at lower redshifts, so the dimming owing to increased luminosity distance is nearly cancelled, and the observed flux is roughly independent of redshift (Lamb & Reichart 2001; Ciardi & Loeb 2000). Second, unlike the spectra of galaxies and quasars, the intrinsic afterglow spectrum of a GRB is a featureless power-law at the relevant wavelengths, allowing a more precise measurement of absorption owing to a neutral IGM (Barkana & Loeb 2004). Finally, since the total star formation is dominated by halos with $m \sim 10^9 M_\odot$ at $z \sim 7$ and because observations at $z \gtrsim 6$ currently probe only the most massive galaxies and QSOs ($m \gtrsim 10^{11} M_\odot$), high-redshift GRB host galaxies should be less massive than those selected in another manner (since the GRB rate likely traces the star formation rate). Consequently, GRB host galaxies will sit in smaller HII regions during reionisation (on average) than galaxies selected by different means, and, therefore, photons near Ly α from a GRB typically suffer enhanced absorption if the IGM is neutral. We show, however, that this final advantage is less significant than previous studies have concluded (e.g., Barkana & Loeb 2004).

In this work, we do not concentrate on wavelengths blueward of source-frame Ly α (in the Ly α forest) to derive constraints from GRBs. Any blueward flux indicates the presence of ionised gas at the redshift of the transmission. However, at high redshifts there is little or no flux in the Ly α forest, even in ionised regions, owing to the increase in density with increasing redshift, the decrease in the size and in the number of voids, and the decrease in the amplitude of the ionising background (e.g., Becker et al. 2007 and Lidz et al. 2007). Moreover, it is difficult to distinguish a partly ionised IGM from a fully ionised one with the $z > 6$ forest (Becker et al. 2007; Lidz et al. 2007). Fortunately, the shape of the line profile redward of Ly α is sensitive to order-unity changes in the neutral fraction of the IGM and, therefore, can be used to unambiguously detect a neutral IGM (Miralda-Escude 1998; Barkana & Loeb 2004).

Little is known about the rate of GRBs at $z > 6$. We assume that the rate of long GRBs traces the massive star formation rate (SFR) for most calculations in this work.² We explain later how we model the massive SFR in our simulations. The assumption that the GRB rate traces the massive SFR is supported by observations of lower redshift GRB host galaxies (Bloom et al. 2002; Djorgovski et al. 2001). However, Kistler et al. (2007) found that the GRB rate is four times higher at $z \approx 4$ than if the GRB rate exactly traces the SFR. Other properties of a galaxy apart from its massive SFR might be correlated with its rate of GRBs. For example, Stanek et al. (2006) found that $z < 0.25$ long GRBs are preferentially in metal-poor galaxies.

² We do not consider the other class of GRBs, the “short” GRBs, in this study. These bursts, while still cosmological, are more local than long GRBs and typically do not have detected afterglow emission.

At $z > 6$, POPIII stars with masses $\sim 100 M_\odot$ may exist in the least massive, least metal-enriched systems. It is unclear whether the death of a POPIII star can result in a GRB. Fryer et al. (2001) identified a mechanism that might produce GRBs from POPIII stars. However, once the interstellar metallicity reaches a critical value of $\sim 10^{-3.5}$ solar in high-redshift galaxies, POPIII star formation quenches and the normal mode of POPII star formation begins (e.g., Mackey et al. 2003; Yoshida et al. 2004), and this mode *is* known to produce GRBs. Most if not all of reionisation likely owes to photons from POPII-like stars (e.g., Sokasian et al. 2003, 2004; Trac & Cen 2006).

In Section 2 we discuss the absorption profiles of a neutral IGM as well as of a damped Ly α absorber (DLA), and, in Section 3, we discuss our simulations of reionisation and their implications for the amount of IGM absorption in a GRB afterglow spectrum. Section 4 quantifies the detectability of a neutral IGM from GRB afterglow spectra, and Section 5 describes the constraints on \bar{x}_H from the $z = 6.3$ burst, GRB050904. For our calculations, we adopt a cosmology with $\Omega_m = 0.27$, $\Omega_\Lambda = 0.73$, $\Omega_b = 0.46$, $\sigma_8 = 0.8$, $n = 1$, and $h = 0.7$, which is consistent with the most recent CMB data (Spergel et al. 2007). We express all distances in comoving units unless otherwise noted.

When this project was nearing completion, we learned of a similar effort by Mesinger & Furlanetto (2007) and refer the reader there for a complementary discussion.

2 THE RED DAMPING WING

In the standard picture, GRB afterglows result from shells of relativistic matter colliding with the interstellar medium, shocking, and radiating via synchrotron emission (Sari et al. 1998). The observed flux of a GRB just redward of rest-frame Ly α is given roughly by $\mathcal{F} = A \nu^{-\beta} \exp[-\tau_\alpha(\nu)]$, where A is the time-dependent amplitude, β is a time-dependent power-law index, and

$$\begin{aligned} \tau_\alpha(\nu) \approx & \int_0^{z_g} \frac{dz}{1+z} \frac{c}{H(z)} n_H(z) \sigma_\alpha \left(\nu_z \left(1 + \frac{v(z)}{c} \right) \right) \\ & + N_{\text{HI}} \sigma_\alpha \left(\nu_{\text{zDLA}} \left(1 + \frac{v(\text{zDLA})}{c} \right) \right). \end{aligned} \quad (1)$$

Here, $\nu_z \equiv \nu (1+z)$, z_g [z_{DLA}] is the redshift of the GRB host galaxy [DLA], ν_α is the frequency at the Ly α line center, $\sigma_\alpha(\nu)$ is the Lorentzian-like Ly α naturally broadened scattering cross section at frequency ν , and $v(z)$ is the line-of-sight peculiar velocity of the gas. The first term on the right-hand side of Equation (1) owes to IGM absorption and the second owes to absorption by a DLA with column density N_{HI} . The absorption profile $\exp[-\tau_\alpha(\nu)]$ yields is commonly referred to as the “damping wing”.

For an isolated bubble of comoving size R_b in a homogeneous medium with neutral fraction \bar{x}_H , ignoring absorption owing to a DLA and the effects of peculiar velocities, Equation (1) simplifies to the expression (e.g., Loeb & Rybicki 1999)

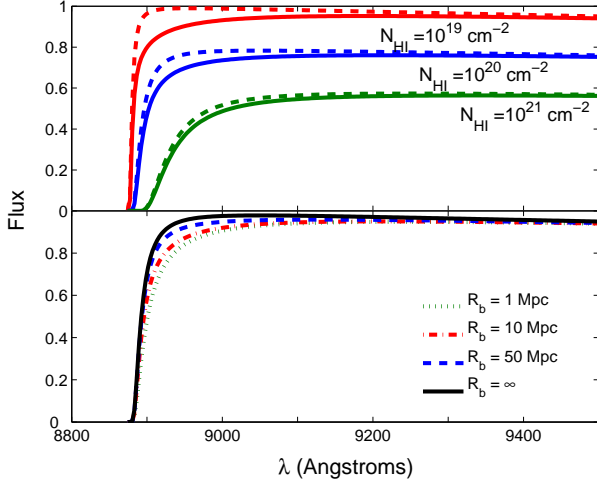


Figure 1. Illustration of the GRB afterglow flux per unit wavelength near Ly α . The top panel depicts the afterglow flux for both an ionised universe (dashed curves) and with $\bar{x}_H = 0.5$ and $R_b = 10$ Mpc (solid curves). The bottom panel illustrates the effect of bubble size on the afterglow flux, assuming $\bar{x}_H = 0.5$ and $N_{\text{HI}} = 10^{20} \text{ cm}^{-2}$. The normalisation of the flux in these panels is arbitrary, and it has been adjusted in the top panel to separate the sets of curves. These curves are calculated with $\beta = 1.25$ and $z_g = 6.3$.

$$\tau_\alpha(\nu) \approx 900 \text{ km s}^{-1} \times \bar{x}_H \left(\frac{1+z_g}{8} \right)^{3/2} \times \left(\frac{H(z_g) R_b}{(1+z_g)} - c \frac{\nu_z - \nu_\alpha}{\nu_\alpha} \right)^{-1}, \quad (2)$$

or $\tau(\nu_\alpha/(1+z_g)) \approx \bar{x}_H$ for a 1 proper Mpc bubble, noting that $H(z_g = 7) \approx 900 \text{ km s}^{-1} \text{ Mpc}^{-1}$.³ The width of the damping wing feature from a neutral IGM (defined here as the $\Delta\lambda$ for which $\exp[-\tau_\alpha(\nu)] < 0.9$) is $\approx 25 (1+z_g) \text{ \AA}$. The width of this feature is typically broader than the feature due to a DLA, which falls off as $\Delta\lambda^{-2}$ rather than the $\Delta\lambda^{-1}$ scaling for IGM absorption, where $\Delta\lambda$ is the difference between a wavelength and Ly α (Miralda-Escude 1998).

Figure 1 illustrates the effect of the column density of the DLA (top panel) and the size of the HII region (bottom panel) on the absorption feature. Here we adopt the same simplistic parameterisation as in Equation (2): an HII region of size R_b surrounded by a homogeneously neutral IGM with neutral fraction \bar{x}_H . The dashed lines in the top panel represent an IGM with $\bar{x}_H = 0$, and the solid lines represent the case with $\bar{x}_H = 0.5$ and $R_b = 10$ Mpc. IGM absorption produces a wider feature than that from a DLA. However, it becomes hard to visually discern absorption owing to a neutral IGM for $N_{\text{HI}} \gtrsim 10^{21} \text{ cm}^{-2}$. This illustration suggests that it is difficult to measure \bar{x}_H from GRB050904, which

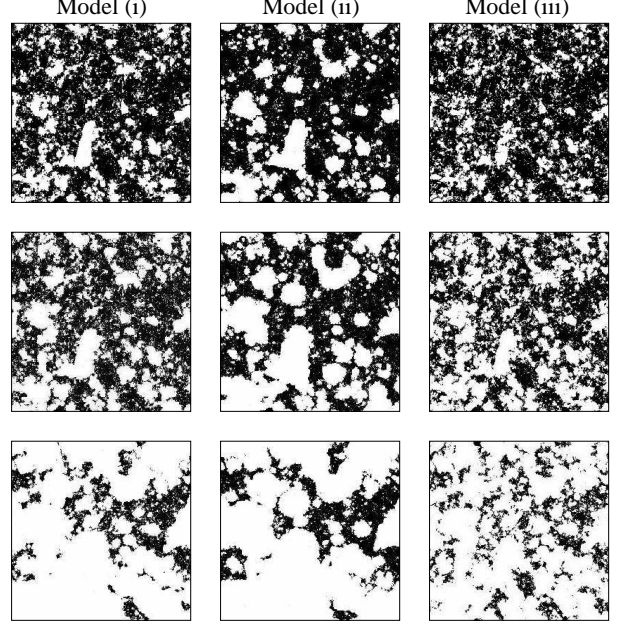


Figure 2. Slices through the middle of the simulation box for the three models discussed in the text, each with width 186 Mpc and with $6.9 < z < 8.5$. The white regions are fully ionised and the black are fully neutral. The top row uses snapshots with volume-weighted neutral fractions of $\bar{x}_{H,V} = 0.7$, the middle uses those with $\bar{x}_{H,V} = 0.5$, and the bottom uses those with $\bar{x}_{H,V} = 0.2$.

has $N_{\text{HI}} \approx 10^{21.6} \text{ cm}^{-2}$ (Totani et al. 2006). We return to this point in Section 5.

DLAs with $N_{\text{HI}} > 10^{19} \text{ cm}^{-2}$ are associated with all but one GRB for which N_{HI} has been measured (Chen et al. 2007). The cumulative distribution of N_{HI} for the current sample of ≈ 30 GRB DLAs scales as $N_{\text{HI}}^{0.3}$ between 10^{18} and $10^{21.5} \text{ cm}^{-2}$ (Chen et al. 2007). About half of all GRBs for which N_{HI} has been measured have $N_{\text{HI}} > 10^{21.5} \text{ cm}^{-2}$ (Chen et al. 2007). However, it is not clear how N_{HI} should scale with redshift. It is plausible that, since halos are less massive at high redshifts, $z > 6$ galaxies should, on average, have weaker DLAs. For galaxies to reionise the Universe, the escape fraction of ionising photons must be appreciable, implying that sight-lines with $N_{\text{HI}} < 10^{18} \text{ cm}^{-2}$ must exist.

The bottom panel in Figure 1 depicts the effect of bubble size on the GRB afterglow spectrum. The IGM absorption for GRBs in bubbles with sizes between 1 – 10 Mpc is comparable. However, if the GRB sits in a large bubble ($R_b \sim 50$ Mpc), the absorption is strongly diminished. When $\bar{x}_H = 0.2$, roughly half of the skewers from GRBs in our reionisation simulations sit in HII regions that are larger than 50 Mpc.

3 EFFECT OF PATCHY REIONISATION

While the GRB itself does not ionise the IGM around it, earlier star formation from its host and neighbouring galaxies can grow a large HII region in the IGM. To model reionisation around a GRB, we employ three radiative transfer simulations that are each 186 Mpc on a side. These simulations are post-processed on a 1024^3 particle N-body

³ To derive Equation (2), we approximate $\sigma_\alpha(\nu)$ with a Lorentzian and ignore the redshift dependence that appears in the numerator of the integrand in Equation (1). We have checked that these approximations are accurate to better than 10% for relevant R_b .

field, assuming that gas traces the dark matter. Unresolved halos are included with extended Press-Schechter merger trees. These three simulations are described in detail in McQuinn et al. (2007b) [and the methodology is described in McQuinn et al. (2007a)], and they are meant to span the range of plausible morphologies for reionisation by galaxies. Here is a brief description of the models for the sources and sinks of ionising photons used in each of the three simulations:

Model (i): All halos above the mass at which the gas can cool atomically (m_{cool}) contribute ionising photons at a rate that is proportional to their mass m . The scaling $\dot{N}_{\text{ion}} \sim m$ assumes that the massive SFR is proportional to the amount of gas within a galaxy.

Model (ii): Halos more massive than m_{cool} contribute to the production of ionising photons, with the ionising luminosity of the sources scaling as halo mass to the 5/3 power. This scaling is chosen to match the relationship between star formation efficiency and galaxy mass that is observed in low-redshift dwarf galaxies (Kauffmann et al. 2003) as well as the SFR found in theoretical studies that include supernova feedback (Dekel & Woo 2003; Hernquist & Springel 2003; Springel & Hernquist 2003).

Model (iii): Absorption by minihalos shapes the morphology of reionisation and $\dot{N}_{\text{ion}} \sim m$ for $m > m_{\text{cool}}$. All minihalos with $m > 10^5 M_{\odot}$ absorb incident ionising photons out to their virial radii until they are photo-evaporated. The photo-evaporation timescale is roughly the sound-crossing time of a halo.

The normalisation of the function $\dot{N}_{\text{ion}}(m)$ in the three simulations is chosen such that reionisation is completed by $z \approx 7$. Given the uncertainties in f_{esc} and the SFR in high-redshift galaxies, there is a large range of possible normalisations. Fortunately, the morphology of reionisation when comparing at fixed \bar{x}_i depends only weakly on the normalisation of \dot{N}_{ion} , as shown in McQuinn et al. (2007a). McQuinn et al. (2007b); McQuinn et al. (2007a) also showed that other effects such as thermal feedback on sub-Jeans mass galaxies, source duty cycle, and the number of recombinations have negligible impact on the morphology for reasonable models. In fact, studies have demonstrated that the morphology of reionisation is shaped principally by the clustering of the ionising sources (Furlanetto et al. 2004a,b, 2005; Zahn et al. 2007; McQuinn et al. 2007a).

Figure 2 displays slices through simulations adopting reionisation models (i), (ii), and (iii). The white regions are ionised and the black are neutral. Model (ii) results in the largest HII regions because it has the most biased sources, whereas model (iii) produces the smallest bubbles, with the maximum bubble radius restricted to be roughly the mean free path for ionising photons to intersect a minihalo.

The absorption profile of a GRB afterglow probes a line of sight through the IGM. Most of the absorption from the IGM occurs at < 70 Mpc from the host galaxy, and the neutral regions closer to the GRB contribute more absorption than those further away. It is clear from Figure 2 that different sight-lines encounter vastly different spatial distributions of x_H . To further illustrate this point, Figure 3 displays nine randomly selected 70 Mpc skewers originating at a GRB in the simulation volume. These skewers are from the $z = 7.3$ snapshot of the simulation using model (i) for

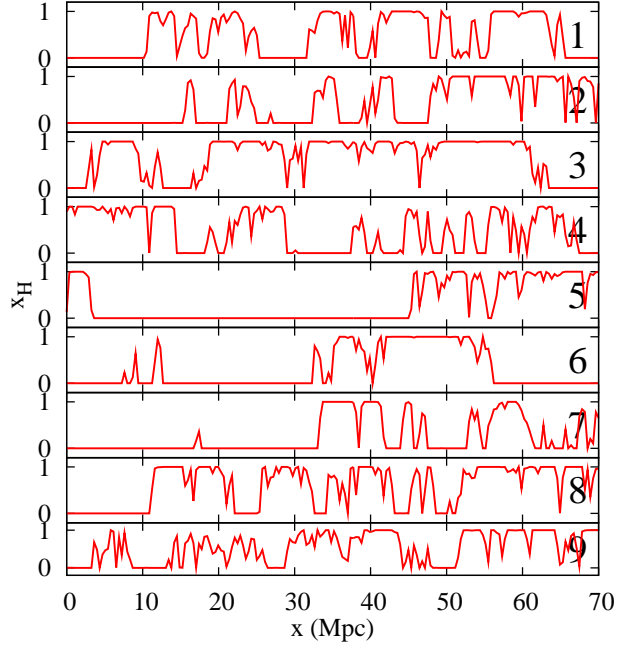


Figure 3. Nine randomly selected 70 Mpc skewers originating at a GRB in the simulation volume. These sight-lines are chosen from a snapshot from the simulation of model (i) that has $\bar{x}_{H,V} = 0.5$ ($\bar{x}_{H,M} = 0.4$) and is from $z = 7.3$.

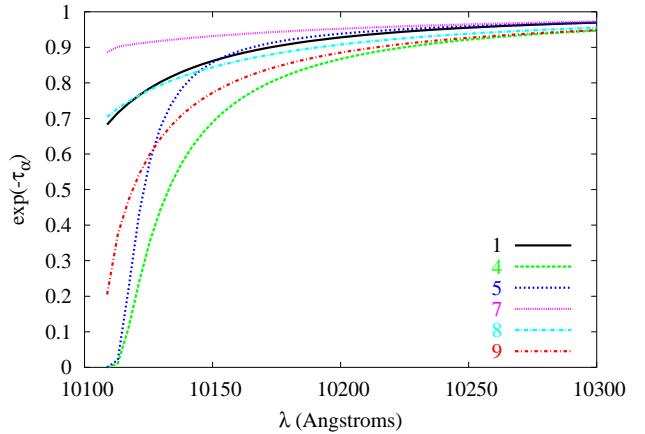


Figure 4. Transmission for six of the nine skewers displayed in Figure 3. Each transmission curve is calculated from the sight-line in Figure 3 that bears the same number.

which the volume-averaged neutral fraction is $\bar{x}_{H,V} = 0.5$ (and mass-weighted neutral fraction is $\bar{x}_{H,M} = 0.4$).⁴ To assign locations for GRBs in the simulation volume, we assume that the \dot{N}_{ion} of a halo is proportional to the GRB rate (which is true if the GRB rate traces the massive SFR and f_{esc} is independent of halo mass).

⁴ The ionisation fronts are much narrower than our grid size for reionisation by POP-II-like stars (as is assumed in these simulations). Resolution effects smear out the simulation ionisation field, making it deviate from a field of 0s and 1s. This smearing does not appreciably affect the results of the calculations reported here.

Figure 4 plots the IGM transmission redward of Ly α for GRBs viewed along six of the nine sight-lines in Figure 3. To compute these curves, we use Equation (1) and the density, ionisation, and velocity fields from the simulation. The observed transmission across these six lines of sight varies enormously, and this variance needs to be accounted for in measurements of \bar{x}_H using GRBs. These calculations do not account for the evolution in \bar{x}_H along the line of sight owing to light-travel effects, but instead compute the absorption from a skewer using a snapshot that is fixed in time. In the time for light to travel 50 Mpc, the value of \bar{x}_H in the simulations of model (i) changes by 0.06, 0.08, and 0.13 when $\bar{x}_H = 0.7, 0.5$, and 0.2 , respectively. A proper treatment of the evolution of \bar{x}_H along a sight-line would hardly affect our conclusions.

For the nine sight-lines in Figure 3, the best fit (\bar{x}_H, R_b) to the afterglow transmission redward of Ly α are respectively (0.31, 6.6), (0.35, 14), (0.47, 2.3), (0.51, 0), (0.28, 0), (0.21, 10), (0.32, 22), (0.45, 10), and (0.43, 2.5).⁵ While these two parameters do not fully characterise the distribution of \bar{x}_H , the actual value for R_b corresponds roughly to the size given by these fits and the fitted value for \bar{x}_H is within 0.3 of the true volume-weighted value. In reality, a DLA will also affect the damping wing profile, and its absorption must be accounted for simultaneously. We perform such analysis in the following section.

The top left panel in Figure 5 plots the probability distribution of a GRB sitting a distance R_b from the bubble edge along a sight-line through the IGM, $P(R_b)$, where the bubble edge is defined as the distance it requires for a skewer to cross three cells that are more than 1% neutral. The dashed, solid, and dot-dashed curves are $R_b P(R_b)$ for $\bar{x}_{H,V} = 0.2, 0.5$ and 0.7 , respectively. The thick curves are for model (i), and the medium width and thin solid curves respectively adopt model (ii) and model (iii) (shown for only $\bar{x}_{H,V} = 0.5$). These curves demonstrate that the function $P(R_b)$ depends more strongly on \bar{x}_H than on the reionisation model. When $\bar{x}_{H,V} \approx 0.5$, the typical GRB resides in a bubble of size $R_b \approx 10$ Mpc, and when $\bar{x}_{H,V} \approx 0.2$ this number increases to $R_b \approx 60$ Mpc.

The top right panel in Figure 5 shows the distribution of \bar{x}_H along a GRB line of sight at fixed global \bar{x}_H . To create the PDF of measured \bar{x}_H , we generate 10^6 skewers that originate at GRBs in the simulation volume and then tabulate \bar{x}_H from each skewer, weighting points as $1/r^2$ – roughly the same weighting that is relevant to the damping wing optical depth at $\nu_\alpha/(1+z_g)$ (eqn. 2) – and not including points inside the host bubble. The widths of these distributions indicate that a GRB cannot be used to directly measure \bar{x}_H to $\delta\bar{x}_H \approx 0.3$.

It is possible that GRBs occur in only the most massive galaxies (rather than in a typical one, as we have assumed thus far), perhaps because earlier metal enrichment is a prerequisite for a GRB to take place.⁶ If only halos

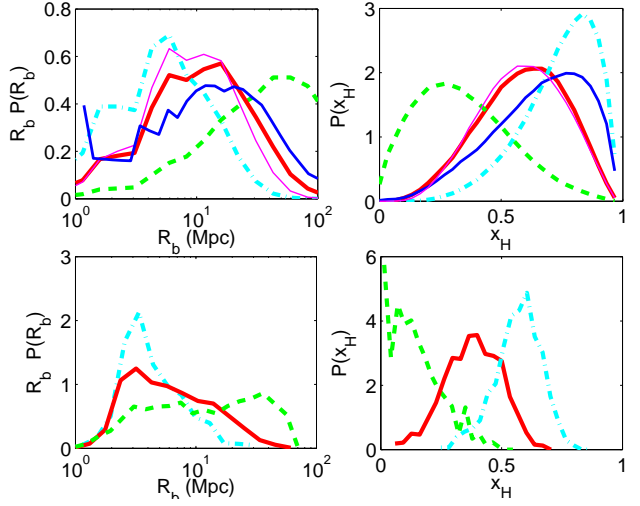


Figure 5. Dashed, solid, and dot-dashed curves represent $\bar{x}_{H,V} = 0.2, 0.5$ and 0.7 , respectively. The thick curves are calculated using model (i), and, in the top panels, the medium width and thin solid curves use model (ii) and model (iii) for $\bar{x}_{H,V} = 0.5$. *Top Left Panel:* The PDF of R_b constructed from 10^6 sight-lines, in which R_b is defined as the length of a skewer originating at a GRB that passes through three cells with $x_H > 0.01$. *Top Right Panel:* The PDF of \bar{x}_H constructed from 10^6 lines of sight, where \bar{x}_H is measured by taking an average of x_H with weighting $1/r^2$ – roughly the weighting that enters τ_α – where r is the distance from the source. Points inside the host bubble are not included in this average. *Bottom Panels:* The same as the top panels except that the PDFs of x_H and R_b are constructed from fitting these parameters to afterglow transmission curves computed from 1000 different simulation sight-lines. DLA absorption is not included in the fitted transmission curves.

with $m > 10^{10} M_\odot$ are able to produce GRBs with a rate proportional to the halo mass, again weighting these halos by their SFR, we find that the average bubble size increases by a comparable amount to the size increase between model (i) and model (ii) shown in Figure 5. This result owes to the bias of the galaxies not changing significantly between $1 \times 10^8 M_\odot$ and $1 \times 10^{10} M_\odot$ as demonstrated by McQuinn et al. (2007a). However, we find that the low-end tail of the $P(R_b)$ starts to disappear with increasing m , even though the peak of the PDF does not shift significantly.

Thus far, we have discussed the distribution of \bar{x}_H and R_b measured directly from the simulations. For a GRB afterglow, \bar{x}_H and R_b are measured by fitting these parameters to the afterglow damping wing (even though this parameterisation for the distribution of x_H along a sight-line is highly simplified). We ignore the effect of DLA absorption in the present calculation, and fit only to the IGM transmission curves. The bottom panels in Figure 5 show the PDF of these parameters from fits to 1000 transmission curves computed from GRBs in the simulation of model (i). The PDFs in the bottom panels are notably different from those in the top panels – favouring smaller R_b and lower \bar{x}_H . While this procedure returns biased values for R_b and \bar{x}_H , we find that

step for a sufficiently energetic jet to be able to emerge from a star to produce a GRB.

⁵ Note that the two skewers which are best fit with $R_b = 0$ are anomalous, and the total fraction of lines of sight that are best fit with $R_b = 0$ is a much smaller fraction than suggested by this sample of nine sight-lines.

⁶ Some metal enrichment may be required for a GRB progenitor to have enough opacity in its photosphere to shed its hydrogen envelope with a wind. This process is thought to be a necessary

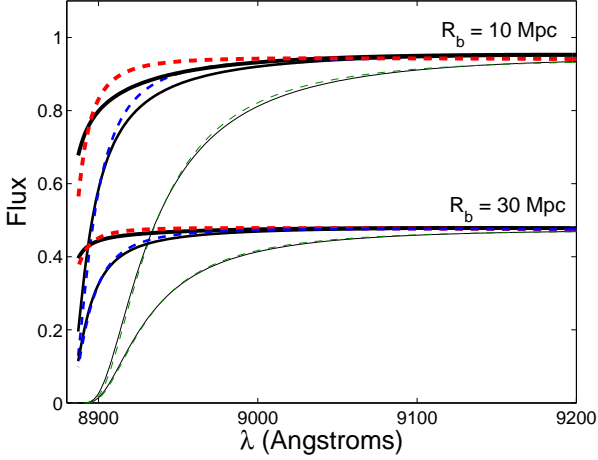


Figure 6. Afterglow spectrum of a hypothetical $z = 6.3$ burst, computed with $\bar{x}_H = 0.5$ and $N_{\text{HI}} = 10^{19} \text{ cm}^{-2}$ (thick solid curves), $N_{\text{HI}} = 10^{20} \text{ cm}^{-2}$ (medium-width solid curves), and $N_{\text{HI}} = 10^{21} \text{ cm}^{-2}$ (thin solid curves) for the specified R_b . The dashed curves are the best fits for a model that assumes an ionised IGM ($\bar{x}_H = 0$) and a DLA, fitted to $\Delta\lambda = 200 (1 + z_g) = 1500 \text{ \AA}$ (a smaller $\Delta\lambda$ results in a better fit). The normalisation of the two sets of curves is adjusted to aid viewing.

this two parameter model provides an excellent fit to the IGM transmission profile (as we discuss in Section 4).

4 FITTING THE DAMPING WING IN GRBS

We would like to quantify the circumstances under which a GRB afterglow can be used to detect a neutral IGM. Previous sections have illustrated how the patchiness of the IGM and the strength of the host DLA complicate this measurement. In addition, there are other uncertainties such as the power-law slope and amplitude of the intrinsic GRB spectrum, the precise redshift of the GRB and of the DLA (which are not always the same), and dust absorption and metal line contamination from the host galaxy or from intervening systems. A systematic discussion of these issues is presented in Totani et al. (2006). To rule out an ionised IGM with a GRB afterglow, a multi-parameter fit to its spectrum assuming an ionised IGM and that accounts for the aforementioned uncertainties must provide a poor fit.

A toy example of such a multi-parameter fit that accounts for some of these uncertainties is shown in Figure 6. Here, we consider the simple case of a bubble with size R_b in a homogeneous IGM with neutral fraction. The solid curves are absorption models that have the intrinsic parameters $\beta = 1.25$, $z_g = z_{\text{DLA}} = 6.3$,⁷ $\bar{x}_H = 0.5$ and $N_{\text{HI}} = 10^{19} \text{ cm}^{-2}$ (thick curves), $N_{\text{HI}} = 10^{20} \text{ cm}^{-2}$ (medium-width curves), or $N_{\text{HI}} = 10^{21} \text{ cm}^{-2}$ (thin curves) as well as the bubble size specified in the figure. Our fitting weights all frequency bins equally, which is a reasonable assumption to

first order. The presence of night-sky OH lines and the wavelength dependence of the CCD sensitivity make the weighting slightly non-uniform in a real observation.

The dashed curves are fits to the parameters N_{HI} , the intrinsic power-law slope β , and the normalisation A of the afterglow flux. The absorption owing to a substantially neutral IGM is more easily fit with just a DLA model as R_b increases or as N_{HI} increases. The fits in Figure 6 assume that z_{DLA} is known from metal lines, as was the case for GRB050904. For GRBs in more metal-poor galaxies or for GRBs with smaller DLAs, this will not always be possible. If fits include z_{DLA} as a free parameter, a neutral IGM is much harder to distinguish from an ionised one (Barkana & Loeb 2004). We include the prior $0.75 < \beta < 1.75$ in the fits: β will likely be constrained by earlier photometric observations redward of the absorption, as was the case for GRB050904 (Totani et al. 2006). In addition, we exclude wavelengths within 400 km s^{-1} of the host galaxy because such regions could be affected by Ly α emission from the galaxy as well as resonant absorption by infalling material.

To quantify the capability of distinguishing different absorption models, we define the measure

$$\langle \Delta\chi^2 \rangle = \sum_{i=1}^N \frac{[F_2(\lambda_i) - F_1(\lambda_i)]^2}{\sigma(\lambda_i)^2}, \quad (3)$$

where F_1 and F_2 are the afterglow fluxes for models 1 and 2. This quantity represents the average difference in χ^2 between two models for a spectrum that has noise $\sigma(\lambda_i)$ in channel λ_i and that has N wavelength channels, assuming the data is drawn from model 1.

When comparing a model with a neutral IGM to an ionised one, we say that two models can be distinguished at X confidence level (C.L.) if X of the total likelihood is contained between the maximum likelihood in the neutral IGM model and $\exp[-\langle \Delta\chi^2 \rangle / 2]$ of that likelihood value (assuming Gaussianity). For a four parameter fit, two models that differ by $\langle \Delta\chi^2 \rangle = 8$ signifies that model 1 is, in the mean, preferred at 91% C.L. over model 2 ($\langle \Delta\chi^2 \rangle = 5$, 70% C.L. and $\langle \Delta\chi^2 \rangle = 12$, 98% C.L.). The significance levels at fixed $\Delta\chi^2$ for fits with five parameters are similar.

We fit to $\Delta\lambda = 50 (1 + z_g) \text{ \AA}$ redward of source-frame Ly α and where the fitted absorption spectrum is parameterised by $N_{\text{HI}} \approx 10^{19} \text{ cm}^{-2}$, $\bar{x}_H = 0.5$, and $R_b = 10 \text{ Mpc}$ (similar to the fits in Fig. 6). The fits result in $\langle \Delta\chi^2 \rangle \approx 5 \times (3 \text{ \AA} / \Delta\lambda) \times (0.1 / \sigma_{\mathcal{F}})^2$ between the model for a neutral IGM and the model for an ionised IGM, where $\Delta\lambda$ is the width of a frequency channel and $\sigma_{\mathcal{F}}$ is the standard deviation in the flux in each channel in units of the normalisation of the intrinsic spectrum, A . The fits to a model with $\bar{x}_H = 0.5$, $R_b = 10 \text{ Mpc}$, and with $N_{\text{HI}} \approx 10^{20} \text{ cm}^{-2}$ [$N_{\text{HI}} \approx 10^{21} \text{ cm}^{-2}$] result in $\langle \Delta\chi^2 \rangle \lesssim 3 [0.2] \times (3 \text{ \AA} / \Delta\lambda) \times (0.1 / \sigma_{\mathcal{F}})^2$. Therefore, $\Delta\lambda \approx 3 \text{ \AA}$ and $\sigma_{\mathcal{F}} \approx 0.1$ are required for any hope of detecting a neutral IGM for the $N_{\text{HI}} \approx 10^{19} \text{ cm}^{-2}$, $\bar{x}_H \approx 0.5$, and $R_b = 10 \text{ Mpc}$ case, and even better sensitivity is required for the other two examples. The Subaru FOCAS spectroscopic observations of GRB050904, which is discussed in Section 5, had $\Delta\lambda \approx 3 \text{ \AA}$ and $\sigma_{\mathcal{F}} \approx 0.1$.

How do the quoted $\langle \Delta\chi^2 \rangle$ depend on the assumptions we have made? For this discussion, we again assume an absorption model with $\bar{x}_H = 0.5$, $R_b = 10 \text{ Mpc}$, and $N_{\text{HI}} \approx 10^{20} \text{ cm}^{-2}$, and we assume a measurement with $\Delta\lambda \approx 3 \text{ \AA}$ and $\sigma_{\mathcal{F}} \approx 0.1$. If we restrict β to $1.0 < \beta < 1.5$

⁷ The assumption that $z_g = z_{\text{DLA}}$ is probably reasonable for high-redshift galaxies, where the circular velocity of these halos is typically $\sim 25 \text{ km s}^{-1}$ (Barkana & Loeb 2004).

(rather than to $0.75 < \beta < 1.75$, as before), $\langle \Delta\chi^2 \rangle$ increases from 3 to 4. If we fix $\beta = 1.25$, then $\langle \Delta\chi^2 \rangle = 5$. In addition, if we allow z_{DLA} to vary and fix $\beta = 1.25$, $\langle \Delta\chi^2 \rangle$ decreases dramatically to 1. Finally, the choice of a bandwidth of $50 (1 + z_g) \text{ \AA}$ also affects the results. If we instead fit the first $200 (1 + z_g) \text{ \AA}$ redward of $\text{Ly}\alpha$, $\langle \Delta\chi^2 \rangle$ increases from 3 to 6. This increase of $\langle \Delta\chi^2 \rangle$ with bandwidth owes to tighter constraints on A and β , which breaks degeneracies between these parameters and the parameters that determine the absorption. The appropriate choice of bandwidth for our calculations is unclear; fits should not include wavelengths where the dust absorption, the instrumental response, and other factors are not understood to better than the difference between the two absorption models. Already for $\Delta\lambda \approx 300 \text{ \AA}$, such calibration is necessary to the 1% level (Fig. 6). In addition, even uncertainties in the cosmological parameters make a difference in distinguishing models at the percent level (Miralda-Escude 1998).

Thus far, we have considered fits to a toy model for IGM absorption. To realistically model IGM absorption and to understand how often a neutral IGM can be detected, we employ skewers from the simulations of model (i) and set $\beta = 1.25$ to calculate the “observed” spectrum. First, we find that a model with R_b and \bar{x}_H (in addition to parameters that account for DLA absorption and the intrinsic afterglow spectrum) typically provides an excellent fit to the data. This is surprising because of the highly simplified nature of this model. The $\langle \Delta\chi^2 \rangle$ between the true model – the absorption profile calculated from the simulation – and the best fit model neutral IGM model (with R_b and \bar{x}_H) typically range between $10^{-3} - 10^{-7} \times (3\text{\AA}/\Delta\lambda) \times (0.1/\sigma_F)^2$ for $N_{\text{HI}} = 10^{20} \text{ cm}^{-2}$. These small values mean that $\sigma_F \approx 10^{-3}$ is required to rule out this model (measurements ≈ 100 times more sensitive than those done on Subaru for GRB050904).

Figure 7 shows the distribution of $\langle \Delta\chi^2 \rangle$ between fits to the simulated spectra using models with R_b , \bar{x}_H , N_{HI} , A and β or with just the last three parameters (i.e., a DLA and an ionised IGM). These fits are to a wavelength interval that spans $50 (1 + z) \text{ \AA}$ redward of rest-frame $\text{Ly}\alpha$. If the fits with $\bar{x}_H = 0$ are disfavoured by the data (i.e., if $\langle \Delta\chi^2 \rangle \gtrsim 8$), then a neutral IGM will be favoured by the data. The parameter y that is plotted on the abscissa in Figure 7 is scaled to be independent of S/N (we define $S/N \equiv \sigma_F^{-1}$) and spectrograph resolution R ($R = \lambda_i/\Delta\lambda_i$, where $\Delta\lambda_i$ is the size of a wavelength channel). For an observation like the one done for GRB050904 ($R = 3000$ and $S/N = 10$), a DLA with $N_{\text{HI}} \lesssim 10^{20} \text{ cm}^{-2}$ is needed to detect a neutral IGM when $\bar{x}_H \approx 0.5$ (left panel in Fig. 7). For $\bar{x}_H < 0.5$, an even better measurement is required.

The results in Figure 7 depend on the parameters we fit as well as the wavelength range included in the fit. If we fix the parameter $\beta = 1.25$ instead of fitting it, the PDFs in this figure are, for the most part, unchanged. If we fit a larger range in wavelength of $\Delta\lambda = 200 (1 + z) \text{ \AA}$, the fits improve slightly – shifting the histogram by factor of ~ 1.5 .

The thin solid curve in the right panel of Figure 7 is the PDF of $\langle \Delta\chi^2 \rangle$ for spectra computed for $\bar{x}_H = 0.5$ and where we have folded in the distribution of N_{HI} observed in lower redshift systems. We assume that the distribution of DLAs is a power-law of the form $N_{\text{HI}}^{0.3}$ for $N_{\text{HI}} < 10^{21.5} \text{ cm}^{-2}$, which is consistent with observations (Chen et al. 2007). Half of GRB DLAs have $N_{\text{HI}} > 10^{21.5} \text{ cm}^{-2}$, but we do not in-

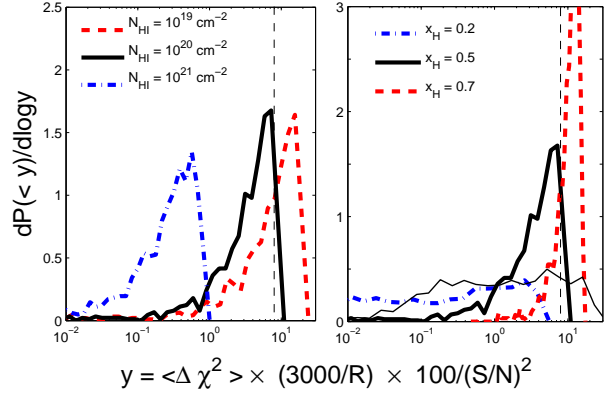


Figure 7. PDF of $\langle \Delta\chi^2 \rangle$ for a spectrograph with $R = 3000$ and $S/N = 10$ in each wavelength channel. $\langle \Delta\chi^2 \rangle$ is the average difference in χ^2 between a model that assumes $\bar{x}_H = 0$ and the “true” model (a model that also fits \bar{x}_H and R_b). We generate this PDF by fitting 1000 sight-lines from the simulation of model (i) at each \bar{x}_H . Note that the parameter y that is plotted on the abscissa is scaled to be independent of S/N and spectrograph resolution, R . The left panel shows the dependence of the PDF on N_{HI} , using spectra from a snapshot with $\bar{x}_H = 0.5$, and the thick curves in the right panel show the dependence on \bar{x}_H , assuming $N_{\text{HI}} = 10^{20} \text{ cm}^{-2}$. The thin black curve in the right panel folds in the observed distribution of N_{HI} and uses spectra from a snapshot with $\bar{x}_H = 0.5$. The fits for the “true” model employ four parameters such that a neutral IGM is detected on average at $> 91\%$ confidence level when $\langle \Delta\chi^2 \rangle > 8$ (marked by the vertical dashed lines for $R = 3000$ and $S/N = 10$).

clude these bursts in this computation. These bursts will contribute to the small $\langle \Delta\chi^2 \rangle$ end of the PDF. Assuming an observation with similar sensitivity to the Subaru FOCAS spectrum of GRB050904, that the distribution of DLAs is the same as found at lower redshift, that the redshift of the GRB is known, a GRB from a redshift at which $\bar{x}_H \approx 0.5$ can be used to detect a partly neutral IGM at 98% C.L. ($\langle \Delta\chi^2 \rangle > 12$) approximately 5% of the time (and, for an observation with 3 times the sensitivity, $\approx 25\%$ of the time) if the fit uses $\Delta\lambda = 50 (1 + z) \text{ \AA}$. If the fit using $\Delta\lambda = 200 (1 + z) \text{ \AA}$, this becomes $\approx 10\%$ of the time (and, for an observation with 3 times the sensitivity, $\approx 30\%$ of the time).

An earlier spectroscopic pointing could result in higher S/N values than the fiducial value of 10 since the optical afterglow fades as a power-law in time with slope ≈ -1.2 (Liang & Zhang 2006). With NIRSpect on JWST, operating in its highest resolution mode ($R = 2700$), to detect a GRB with $S/N = 10$ in each frequency bin requires a minimum flux of $F(\lambda) = 2 \times 10^{-19} \text{ erg cm}^{-2} \text{ s}^{-1} \text{ \AA}^{-1}$ for a 10^4 sec integration for $\lambda \approx 10^4 \text{ \AA}$ ($z \approx 8$).⁸ This minimum flux is approximately five times the sensitivity of the Subaru FOCAS observation of GRB050904. JWST will be able to slew to high-redshift afterglows ~ 1 day after the burst (Gardner et al. 2006). However, from the ground, a near-infrared spectrograph is necessary for higher redshift bursts than GRB050904 (for which the spectrum was taken with

⁸ <http://www.stsci.edu/jwst/instruments/nirspect/>

the optical spectrograph FOCAS), which will result in worse flux sensitivity.

Even though the calculations in this section were for $z \approx 6-8$, similar conclusions hold for higher redshifts reionization scenarios. The amount of absorption does increase with increasing z_g because the damping wing optical depth scales as $\approx (1 + z_g)^{3/2}$. However, the morphology of reionization depends weakly on redshift for stellar reionization scenarios – bubbles have the same comoving size independent of when reionization happens (McQuinn et al. 2007a). For reasonable redshifts over which reionization could occur, the amount of damping wing absorption predicted by our simulations is similar.

As a final point, the distribution of the best-fit R_b and \bar{x}_H from the fits that include DLA absorption are very similar to the distribution in Figure 5 in which the effect of a DLA was ignored. Therefore, the presence of a DLA does not significantly bias the best fit values for R_b and \bar{x}_H .

5 GRB050904

The $z = 6.3$ GRB, GRB050904, is the burst with the highest identified redshift (Kawai et al. 2005; Haislip et al. 2006; Totani et al. 2006). An optical afterglow spectrum of this burst was taken using the FOCAS instrument on Subaru with a 4 hr observation 3.4 days after the prompt gamma ray emission. Totani et al. (2006) showed that this spectrum is well-fitted with a DLA of column density $N_{\text{HI}} \approx 10^{21.6} \text{ cm}^{-2}$ and that this GRB disfavors additional absorption owing to a neutral IGM at $z = 6.3$.

We have re-performed the analysis of Totani et al. (2006), accounting for galactic absorption of $E(B - V) = 0.06$ and masking the same regions of the spectrum as in Totani et al. (2006) because of metal line contamination. (The thick horizontal lines at the top of Figure 8 indicate the wavelength ranges that were fit.) The solid absorption curve in Figure 8 is the best fit for an ionised IGM ($\bar{x}_H = 0$) with a DLA and the dashed curve is the best fit with a DLA plus a fully neutral IGM ($\bar{x}_H = 1$). Both fits employ the same estimated errors as in Totani et al. (2006) and minimise χ^2 with two parameters, N_{HI} and A , holding all other parameters fixed. In particular, we fix $\beta = 1.25$ as was done in Totani et al. (2006). This value for β is consistent with $\beta = 1.25 \pm 0.25$, which was derived in Tagliaferri et al. (2005) from photometric observations 1.2 days after this burst. Totani et al. (2006) argued that the softness of the β derived in Tagliaferri et al. (2005) indicates that β was determined by the power-law index of the electrons and, therefore, should not evolve significantly between the time of the measurement from Tagliaferri et al. (2005) and their measurement (i.e., other breaks in the synchrotron spectrum are at longer wavelengths). The value of $\Delta\chi^2$ is not significantly changed if we instead fit with β adopting the prior $1.0 < \beta < 1.5$ (the best fit for both models then prefers $\beta = 1$).⁹

⁹ If we ignore photometric constraints on β and just fit it as a free parameter, the ionised IGM model prefers $\beta = -0.6$ at 98% C.L. ($\Delta\chi^2 = 10$) over a model with $\beta = 1.25$. While it is hard to imagine β evolving to this small value from $\beta = 1.25$, this nevertheless may indicate that there is a problem with the model

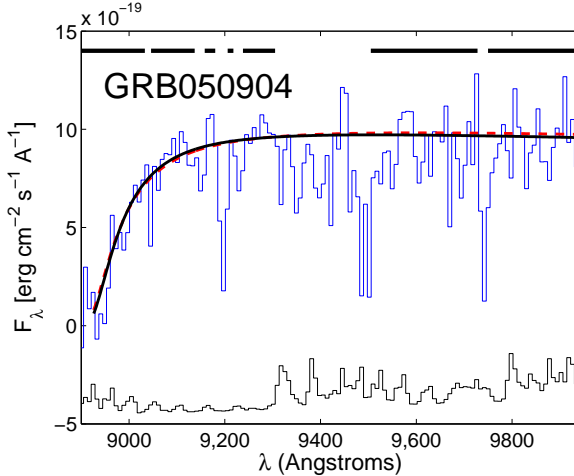


Figure 8. Binned afterglow spectrum of GRB050904 (each 2.67 \AA wavelength channel has been binned into 8 \AA pixels), as well as the best fit models for $x_H = 0$ (solid curve) and $x_H = 1$ (dashed curve). The bottom curves are the $1\text{-}\sigma$ errors on each binned pixel with an offset of -5×10^{-19} , and the thick horizontal lines at the top of the figure indicate the wavelengths that were included in the fits. Both fits require a DLA with column density $N_{\text{HI}} \approx 10^{21.5} \text{ cm}^{-2}$.

The χ^2 values for the two models displayed in Figure 8 are 277.3 for the ionised model and 287.0 for the neutral case.¹⁰ Even though these two 3-parameter models are difficult to distinguish visually, it is the case that $\Delta\chi^2 = 9.7$, which at face value implies that the ionised model is preferred over the neutral model at 98% C.L. (Totani et al. 2006). Interestingly, much of the contribution to $\Delta\chi^2$ between the neutral and ionised models comes from wavelengths that are not significantly affected by IGM and DLA absorption. If we tabulate $\Delta\chi^2$ for the best fit models in Figure 8, only including the wavelengths within 200 \AA of $\text{Ly}\alpha$ – the wavelengths most affected by absorption – in the summation, the two model fits differ by $\Delta\chi^2 = 4$. If we include 700 \AA redward of $\text{Ly}\alpha$, the two model fits in Figure 8 differ by $\Delta\chi^2 = 5$. The significant contribution to $\Delta\chi^2$ from redward of the $\text{Ly}\alpha$ absorption stems from the fact that the neutral IGM model prefers a 2.4% higher normalization to compensate for the additional effect of IGM absorptions. As a consequence, the unabsorbed part of the spectrum needs to be modelled to a relative precision of a percent over a wavelength range with $\Delta\lambda/\lambda \approx 0.1$ for a correct interpretation of the data.

To distinguish models that differ at the 2% level over hundreds of angstroms posits that intergalactic metal and

for the data. Fits to the spectrum that do not place a prior on β do not prefer ionised IGM models over neutral ones.

¹⁰ To emulate the results of Totani et al. (2006), the error bars have been renormalised by the factor of 0.848 from their originally estimated value such that the $\chi^2/\text{d.o.f.} \approx 1$ for the best fit ionised model, where the number of degrees of freedom (d.o.f.) equals $268 - 3$. Totani et al. (2006) uses this rescaling to correct for uncertainty in the errors. The residuals for the best fit ionised model are close to a Gaussian with the correct width after this procedure (Fig. 3 in Totani et al. 2006).

sky lines have been properly masked, that the dust reddening of the Milky Way and the host galaxy has been accurately accounted for, that the relative calibration of and errors on the measured flux are accurate, and that the model for the intrinsic spectrum is correct. Totani et al. (2006) investigated many of these uncertainties and argued that the FOCAS spectrum of GRB050904 can be used to distinguish the models in Figure 8.

It is unlikely that the IGM is more than half neutral at $z = 6.3$ given that high-redshift quasars reveal that it is fully ionised at $z \lesssim 6$ (Lidz et al. 2007). However, while GRB050904 may favour an ionised universe over a neutral universe, it is more difficult to place a constraint on intermediate \bar{x}_H with GRB050904, especially in light of the large bubble sizes during reionization. For example, if we fit a model that fixes $\bar{x}_H = 0.5$ and $R_b = 10$ Mpc [30 Mpc] – again fitting with A and N_I and fixing β –, then the $\Delta\chi^2$ between a model with an ionised universe and this model is 3.1 [2.5], which is not statistically significant.

6 THE DAMPING WING IN QSOS AND GALAXIES

GRBs are not the only beacons in which the signature of a neutral IGM can be observed in their continuum emission. Rather than wait for a high-redshift GRB to occur, hundreds of $z > 6$ galaxies and QSOs have already been found – perhaps such objects can be used to detect a neutral IGM. However, since the observed QSOs and galaxies are more biased tracers of the high-redshift Universe than are GRBs (assuming GRBs trace star formation), they sit in larger bubbles such that the damping wing absorption is smaller, on average. The effective size of an HII region for one of the known $z \approx 6$ quasars, assuming that the IGM is significantly neutral at this redshift, is probably > 50 Mpc. This number accounts for these rare objects being in the most overdense regions in which reionisation occurs earlier (Lidz et al. 2007). Such large HII regions make searches that target the red damping wing in the highest redshift quasars hopeless.¹¹

Galaxies will sit in smaller HII regions than QSOs. The average bubble size around galaxies is slightly larger than those for GRBs, which for spectroscopically confirmed galaxies currently have $m \approx 10^{10-11} M_\odot$ (e.g., McQuinn et al. 2007b). As noted in §3, the difference in the typical bubble size is typically less than a factor of two between halos of $m \approx 10^{10-11} M_\odot$ and GRB-hosting halos.

However, there are two significant complications for using galaxies over GRBs. First, the continuum emission for high-redshift galaxies is difficult to detect spectroscopically with existing facilities. Stacking galaxy spectra is necessary to have any hope of detecting a damping wing feature with current data. Another significant complication is that the continuum of galaxies is not a simple power-law, nor is the

effect of N_{HI} as simple as for a GRB. For example, there is not a unique N_{HI} for a galaxy since star formation is occurring at many places in the galaxy. Such uncertainties must be accounted for in any analysis that attempts to obtain \bar{x}_H from the damping wing absorption profile of a galaxy.

7 CONCLUSIONS

GRBs are the most luminous sources at high redshifts, and their smooth power-law spectra are ideal for isolating the effects of absorption owing to a neutral IGM. However, observations must be able to separate the impact of IGM absorption from that of a DLA to detect a neutral IGM. If no damping wing feature from IGM absorption is detected in the spectrum of a high-redshift GRB, one must be careful to conclude that reionisation is complete at the redshift of interest.

We have shown that there is a wide probability distribution of HII region sizes, and that there is large variation in the distribution of \bar{x}_H along different sight-lines. A non-detection of neutral hydrogen from a GRB afterglow spectrum might arise merely because the GRB host galaxy sits within a large HII region. If absorption owing to a neutral IGM is detected, it will be impossible to infer \bar{x}_H from a single GRB to better than $\delta\bar{x}_H \sim 0.3$ because of the patchiness of reionisation.

Assuming an observation with similar sensitivity to the Subaru FOCAS spectrum of GRB050904, that the distribution of DLAs is the same as found at lower redshift, and that the redshift of the GRB is known, a GRB from a redshift at which $\bar{x}_H \approx 0.5$ can be used to detect a partly neutral IGM at 98% C.L. $\approx 5 - 10\%$ of the time (and, for an observation with 3 times the sensitivity, $\approx 25 - 30\%$ of the time). Constraints from GRBs occurring at epochs with smaller \bar{x}_H result in an even smaller fraction of GRBs yielding detections of a neutral IGM. Weaker DLAs enhance the probability of detecting a neutral IGM, but too weak of a DLA may prevent a precise redshift determination.

Since the $z = 6.3$ burst GRB050904 has a DLA with $N_{\text{HI}} = 10^{21.6} \text{ cm}^{-2}$, the absorption on the red side of the line is dominated by the DLA (Totani et al. 2006). While this burst may favour a model with an ionised universe over a neutral universe (Totani et al. 2006), a weaker DLA is necessary to be able to precisely constrain \bar{x}_H in the spectrum of a high-redshift GRB.

GRB050904 was observed spectroscopically by the Subaru telescope 3.4 days after the prompt gamma ray emission. If this afterglow had been observed hours after the burst, the flux would have been more than an order of magnitude larger. To detect a neutral IGM, it is crucial for optical and near-infrared spectrographs to observe candidate high-redshift GRBs as soon as possible after the prompt gamma ray emission, since a high signal-to-noise ratio is necessary to distinguish IGM absorption from that arising from a DLA. Such an observing programme is worthwhile given the promise that GRBs have as probes of the epoch of reionisation.

¹¹ Rather than analyse wavelengths redward of the QSO Ly α line, damping wing absorption from neutral patches in the IGM would also affect the Ly α forest of these QSOs (Mesinger & Haiman 2007). Owing to little forest transmission at $z > 6$, this feature would be difficult to detect (Lidz et al. 2007).

8 ACKNOWLEDGMENTS

We would like to thank T. Totani for providing the Subaru afterglow data for GRB050904 as well as for answering numerous questions about the measurement. We also thank Mark Dijkstra, Claudé-Andre Faucher-Giguère, Alexandre Tchekhovskoi, and Hy Trac for many interesting discussions. MM acknowledges support through an NSF graduate student fellowship. The authors are also supported by the David and Lucile Packard Foundation, the Alfred P. Sloan Foundation, and grants AST-0506556 and NNG05GJ40G.

REFERENCES

- Barkana R., Loeb A., 2004, *ApJ*, 601, 64
- Becker G. D., Rauch M., Sargent W. L. W., 2007, *ApJ*, 662, 72
- Bloom J. S., Kulkarni S. R., Djorgovski S. G., 2002, *AJ*, 123, 1111
- Chen H.-W., Prochaska J. X., Gnedin N. Y., 2007, *ArXiv e-prints*, 707
- Ciardi B., Loeb A., 2000, *ApJ*, 540, 687
- Dekel A., Woo J., 2003, *MNRAS*, 344, 1131
- Djorgovski S. G., et al., 2001, in Costa E., Frontera F., Hjorth J., eds, *GRBs in the Afterglow Era*. pp 218–+
- Filliatre P., et al., 2006, *A&A*, 448, 971
- Fryer C. L., Woosley S. E., Heger A., 2001, *ApJ*, 550, 372
- Furlanetto S. R., McQuinn M., Hernquist L., 2005, *MNRAS*, pp 1043–+
- Furlanetto S. R., Zaldarriaga M., Hernquist L., 2004a, *ApJ*, 613, 1
- Furlanetto S. R., Sokasian A., Hernquist L., 2004b, *MNRAS*, 347, 187
- Gardner J. P., et al., 2006, *Space Science Reviews*, 123, 485
- Grindlay J. E., The Exist Team 2006, in Holt S. S., Gehrels N., Nousek J. A., eds, *GRBs in the Swift Era Vol. 836 of AIP Conference Series*. pp 631–641
- Haislip J. B., et al., 2006, *Nature*, 440, 181
- Hernquist L., Springel V., 2003, *MNRAS*, 341, 1253
- Kawai, N., et al. 2005, *ArXiv Astrophysics e-prints*, arXiv:astro-ph/0512052
- Kauffmann G., et al., 2003, *MNRAS*, 341, 33
- Kistler M. D., Yuksel H., Beacom J. F., Stanek K. Z., 2007, *ArXiv e-prints*, 709
- Lamb D. Q., Reichart D. E., 2001, *astro-ph/0109037*
- Liang E., Zhang B., 2006, *ApJL*, 638, L67
- Lidz A., McQuinn M., Zaldarriaga M., Hernquist L., Dutta S., 2007, *astro-ph/0703667*
- Loeb A., Rybicki G. B., 1999, *ApJ*, 524, 527
- Mackey J., Bromm V., Hernquist L., 2003, *ApJ*, 586, 1
- Malesani, D., Covino, S., Rossi, E. M., Lazzati, D., de Luca, A., Filliatre, P., & Tagliaferri, G. 2005, *Nuovo Cimento C Geophysics Space Physics C*, 28, 515
- McQuinn M., Lidz A., Zahn O., Dutta S., Hernquist L., Zaldarriaga M., 2007a, *MNRAS*, 377, 1043
- McQuinn, M., Hernquist, L., Zaldarriaga, M., & Dutta, S. 2007b, *MNRAS*, 797
- Mesinger A., Haiman Z., 2007, *ApJ*, 660, 923
- Mesinger A., Furlanetto S. R., 2007, *astro-ph/0710.0371*
- Miralda-Escude J., 1998, *ApJ*, 501, 15
- Sari R., Piran T., Narayan R., 1998, *ApJL*, 497, L17+
- Sokasian A., Abel T., Hernquist L., Springel V., 2003, *MNRAS*, 344, 607
- Sokasian A., Yoshida N., Abel T., Hernquist L., Springel V., 2004, *MNRAS*, 350, 47
- Spergel D. N., et al., 2007, *ApJS*, 170, 377
- Springel V., Hernquist L., 2003, *MNRAS*, 339, 312
- Stanek K. Z., et al., 2006, *Acta Astronomica*, 56, 333
- Tagliaferri G., et al., 2005, *A&A*, 443, L1
- Totani T., Kawai N., Kosugi G., Aoki K., Yamada T., Iye M., Ohta K., Hattori T., 2006, *PASJ*, 58, 485
- Trac H., Cen R., 2006, *astro-ph/0612406*
- Yoshida N., Bromm V., Hernquist L., 2004, *ApJ*, 605, 579
- Zahn O., Lidz A., McQuinn M., Dutta S., Hernquist L., Zaldarriaga M., Furlanetto S. R., 2007, *ApJ*, 654, 12